Performance Comparison of a Transpired Air Solar Collector with Low-E Surface Coating

Stephen Harrison[1], Anh Kiet Nguyen[2], Gary Johnson[2] and Lucio Mesquita[3]

[1] Queen's University, Mechanical and Materials Engineering, Kingston (Canada)

[2] QSBR Innovations, Kingston (Canada)

[3] Natural Resources Canada, CanmetENERGY-Ottawa, Ottawa (Canada)

Abstract

Transpired air solar collectors are often used to preheat ventilation-air in commercial buildings. Outdoor air is drawn through a perforated, unglazed metal absorber and delivered to a building space in a single pass. Until recently, high-emittance absorber coatings were commonly used, making them susceptible to radiant thermal losses to the surrounding environment. The recent development of durable, low-emittance coatings has allowed manufacturers to offer these surfaces on their unglazed products. This study compares the performance of two transpired solar air collectors: one with a high-emittance absorber coating and the other with a low-emittance coating. Results indicate that, the low-emittance surface coating significantly increased both the efficiency and delivery air temperature compared to the collector with the high-emittance surface coating.

Keywords: Unglazed Transpired Solar Air Collector, Low-emittance Absorber

1. Introduction

The use of transpired solar collectors to preheat ventilation-air represents one of the most cost-effective solar energy applications. Primarily used on commercial buildings, outdoor air is drawn through a perforated, unglazed metal absorber and delivered to a building space in a single pass (Badache et al. 2013). Until recently, high-emittance absorber coatings were commonly used, making them susceptible to radiant thermal losses to the surrounding environment. However, the development of durable, low-emittance coatings has allowed manufacturers to offer these surfaces on their unglazed products. This study compares the thermal performance of two transpired solar air collectors: one with a high-emittance surface coating as a baseline and the other with a highly spectrally selective low-emittance coating.

Geometrically identical collector samples were installed side-by-side on a south-facing vertical wall and operated under natural environmental conditions during 2023 and 2024's winter. Both collectors were operated under typical airflow conditions, and ambient and collector temperatures, incident solar energy and wind intensity were monitored in real-time. *Shukla et al (2012) reviewed the state-of-the-art of the technology.*

2. Description of Experimental Measurements

Geometrically identical collector samples were installed side-by-side on a south-facing vertical wall and operated under natural environmental conditions during the winter of 2023 and 2024. Both collectors were operated under typical airflow conditions, and ambient and collector temperatures, incident solar energy and wind intensity were monitored in real-time.

2.1 Test Samples

The two collectors used in the test were constructed of commercially available, unglazed transpired solar thermal air collector panels with perforated aluminum absorber plates. The panels were attached to identical insulated boxes specially constructed by the manufacturer for this study. The assembled test samples were identical except for the surface coatings. One used a non-selective painted surface (SRCC, 2016), and the other,

Selection and/or peer review under responsibility of Scientific Committee
10.18086/eurosun.2024.07.14 Available at http://proceedings.ises.org

a (0.025) low-emittance surface coating, (SRCC, 2020; Fraunhofer, 2020). The thermal-optical properties and dimensions of the two samples tested are given in Table 1. Figure 1 shows the cross-section profile dimensions of the test samples' absorber sheets. A close-up view of the absorber surface of the selective absorber surface showing the surface perforations for airflow is shown in Figure 2. Both collector samples had identical absorber geometries and perforations.

The collectors were mounted vertically on a south-facing wall, Fig. 3. A 5 cm rigid foam insulation was placed behind each collector to reduce heat loss through the back surface.

Tab. 1: Properties of samples tested

Sample	Absorptance, α	Emittance, ε	Base material (0.75 mm thick)	Dimensions (L x W x H)
Selective	0.935	0.025	Perforated Aluminium sheet	2.44 x 1.03 x 0.20 (m)
Non-selective	0.95	0.95*	Perforated Aluminium sheet	2.44 x 1.03 x 0.20 (m)

*Note. Estimated value

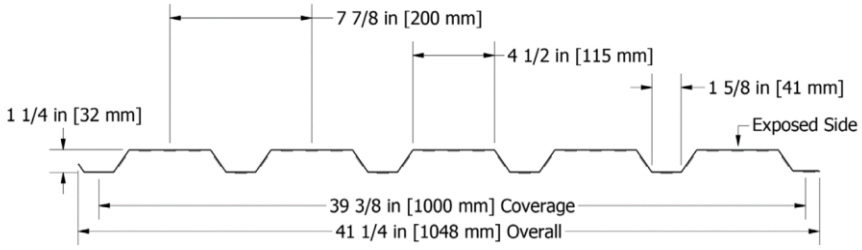

Fig. 1: Cross-section profile dimensions of the test samples' absorber sheets

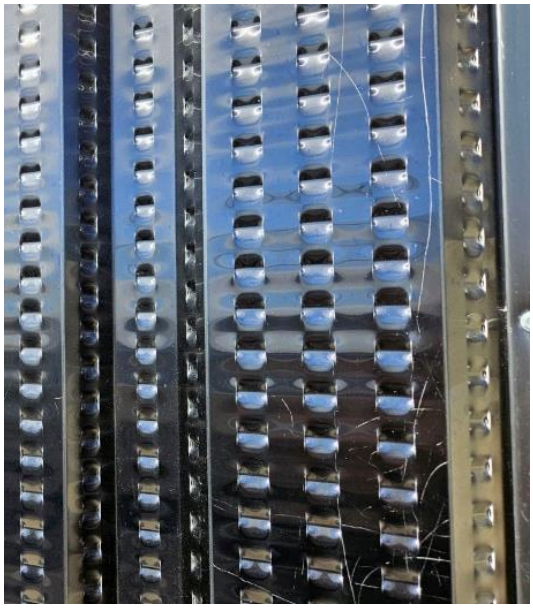

Fig. 2: A close-up view of the absorber surface showing the surface perforations for airflow

Fig. 3: Collectors mounted vertical on the building's south-facing wall.

2.2 Experimental Configuration and Instrumentation

During testing, the collectors were mounted vertically on a south-facing wall at the Solar Calorimetry Laboratory, Queen's University, located in Kingston Ontario. Canada (44.23° N, 76.49° W). The geometrically identical collector samples were installed side-by-side on a south-facing vertical wall and operated under natural environmental conditions during the winter of 2023 and 2024. Both collectors were operated under the same airflow conditions. Ambient and collector temperatures, collector volumetric flowrate, incident solar energy, barometric pressure and wind intensity were monitored in real-time.

Each solar collector sample was connected to a separate air-flow circuit, instrumented to measure the instantaneous power output of each sample, Fig. 4. All instrumentation had current calibration certifications, traceable to secondary standards. During operation ambient air was drawn through the collectors" perforated absorber plates by centrifugal blowers. Various flowrates could be set by varying the blower's speed using variable frequency (VFD) controls.

Air exited each solar collector through a 10 cm diameter opening located at its top-center, through the wall and into a blower. Inside the building, temperature & humidity sensors and laminar flow elements were used to measure collected energy.

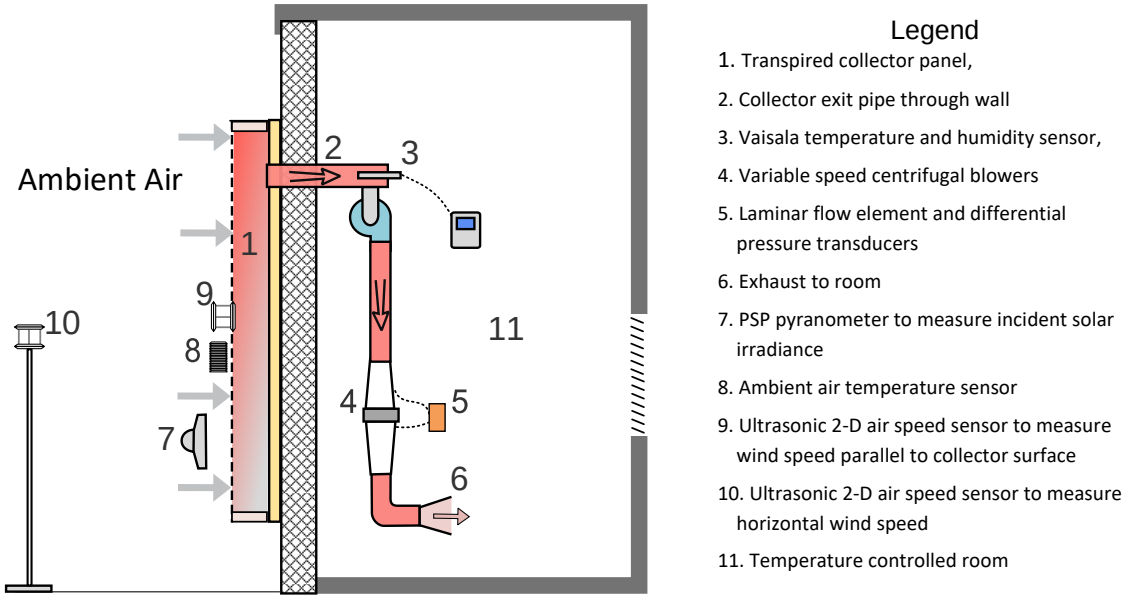

Fig. 4: Schematic of the of one of the test flow circuits showing monitoring points

With this setup, the incoming air was directed through the sensors and the laminar flow element, and into a temperature-controlled space, Fig. 4. Two pyranometers were mounted vertically between the collectors to measure solar radiation and two ultrasonic wind transducers were mounted vertically, parallel with the collector surface. An additional ultrasonic sensor was mounted in front of the collectors, to measure ambient air temperatures, wind speeds, and wind direction. In addition, there was a propeller anemometer placed approximately 15 m from the collectors to measure the overall wind speed at the test location.

All experimental data for both systems was recorded in real time ever 30 seconds with a Campbell Scientific CR1000 data acquisition system. Campbell Scientific data acquisition software Loggernet IV® was used to process and display the data in real time, Fig. 5.

The collectors were monitored over multiple days and weather conditions during the months of March and April 2023, and the winter of 2024. The two collectors were set to run at different air flow rates consisting of 45 CFM, 80 CFM, 105 CFM, and 185 CFM. Data collected during this time was analyzed to compare the thermal performance of the non-selective and selective surface collectors.

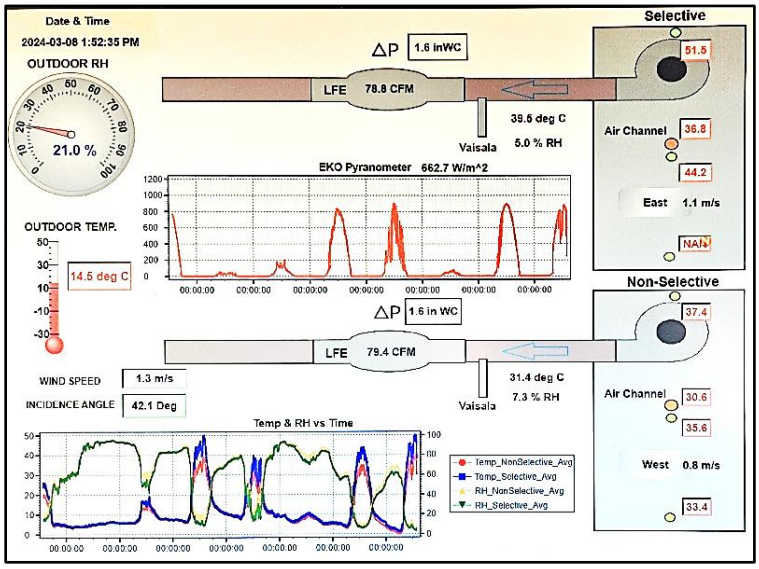

Fig. 5: Screenshot of data monitoring software

3. Results & Discussions

3.1 Analyses of Results

Tests were performed from the 18th of December 2023 to the 24th of March 2024. During the monitoring period, the flowrate through the collectors was adjusted to investigate the effects of array flow rate and suction velocity through the absorber surface. To compare the performance of the solar collectors, the raw data for each collector was processed in MS Excel to determine the instantaneous power output over the course of daylong periods and to determine the total energy delivered during the day. Values of instantaneous and average daily efficiency were calculated. To determine the solar collector net power output, $\dot{Q}_{col}$ was calculated accounting for positive or negative heat gain through the back wall of the building, i.e.,

$$\dot{Q}_{col} = \left(\dot{m} \cdot Cp_m \cdot \Delta T \right) \text{(W)} \qquad \text{(eq. 1)}$$

where $\dot{m}$ is the air mass flowrate (kg s^{-1}),

Cp_m = Specific heat capacity of moist air (kJ $kg^{-1}K^{-1}$)

$$\Delta T = T_{out} - T_a, \text{ (K)} \qquad \text{(eq. 2)}$$

where T_{out} is the temperature of the air exiting the collector (°C), and

T_a is the temperature of the ambient air entering the collector (°C).

The values of Cp_m, $\dot{m}$ and the density of air were calculated at the average temperature of the air entering and exiting the solar collectors.

Daily values of collected energy were calculated by numerically integrating the measured data over the course of daylong periods, i.e.,

$$Q_{day} = \frac{1}{1000} \cdot \int_{sunrise}^{sunset} \dot{Q}_{col}\, dt \qquad \text{(eq. 3)}$$

where Q_{day} is the total solar energy delivered to the building over a daylong period in kJ or expressed in kWh as

$Q_{day,kWh} = Q_{day} / 3600$.

The instantaneous efficiency (expressed as a percentage) for the solar collector was calculated as:

$$\eta_{wall} = 100 \cdot \frac{\dot{Q}_{col}}{(G_i) * A_{col}} \qquad \text{(eq. 4)}$$

where G_i = Total incident solar radiation on the surface of the collector (W m^{-2}), and

The daily efficiency for the solar collector wall was calculated as a percentage, i.e.,

$$\eta_{daily} = 100 \cdot \frac{Q_{day}}{(H_i/1000) * A_{col}} \qquad \text{(eq. 5)}$$

where H_i is the total irradiance striking surface of the solar collectors' absorber over the course of a day in J m^{-2}.

3.2 Experimental Results

Day-long periods were selected from the full data set for detailed analysis and the results. Example plots of power output for each collector non-selective (high-emittance) and selective absorbers (low-emitance) are plotted for both a clear and overcast day in Fig. 3 and Fig. 4.

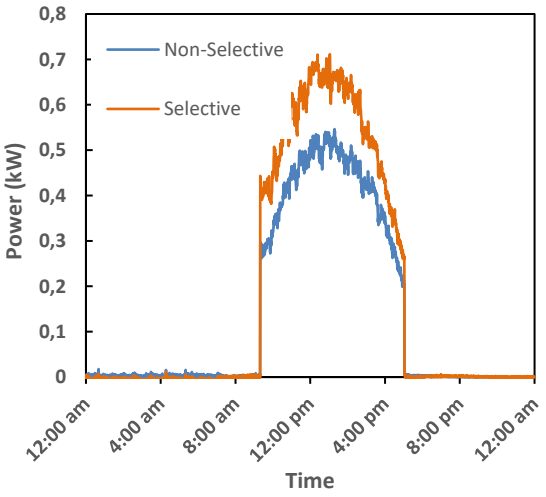

Fig. 6: Delivered Power vs Time for Clear Sky Day, April 1st, 2023, ambient air temperature = 4ºC, (9:00 am to 5:00 pm)

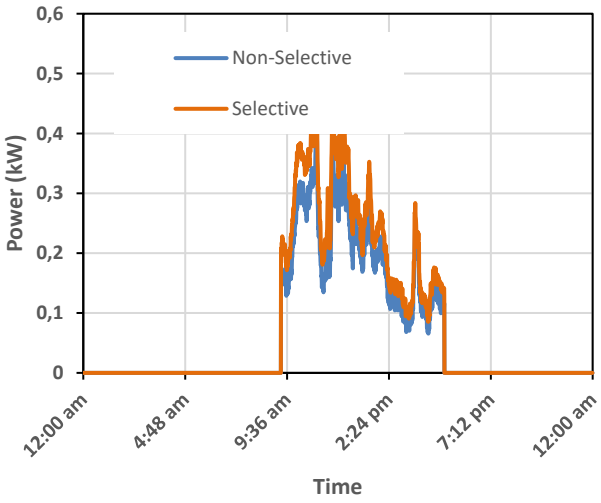

Fig. 7: Delivered Power vs Time for Cloudy Day, April 11, 2023, ambient air temperature = 8ºC, (9:00 am to 5:00 pm)

To evaluate how the selective and non-selective solar collectors performed, the daily energy delivered by the two collectors was compared under four different flow rates: 45 CFM, 80 CFM, 105 CFM, and 185 CFM. Plots showing the daily energy delivered by each of the collectors is compared for different air flow rates are shown below in Figs. 8 to Fig. 15. The ratio of the energy delivered by the low-emittance collector relative to the non-selective collector are also shown

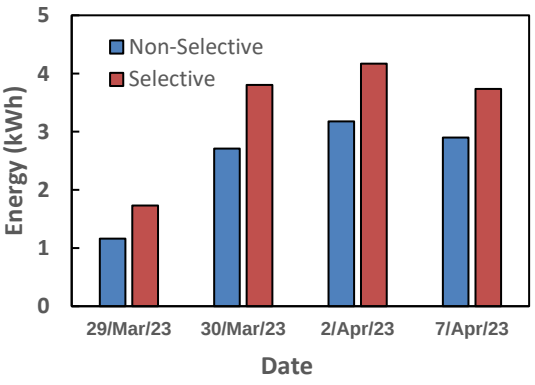

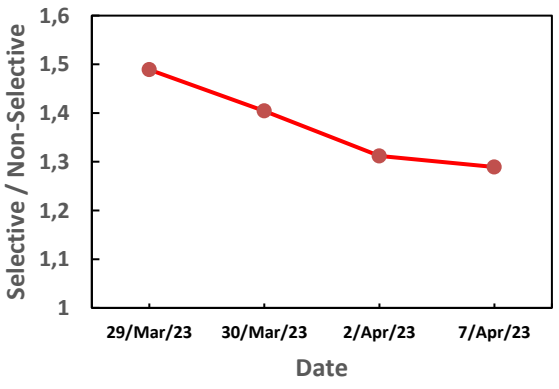

Fig. 9: Ratio of daily energy delivered for collector with selective absorber coating (i.e., low-emittance) relative to the non-selective (i.e., high-emittance)

Fig. 8: Comparison of collector energy delivered per day at 0.02 m^3s^{-1} (45 CFM) or 0.0084 $m^3s^{-1}m^{-2}$

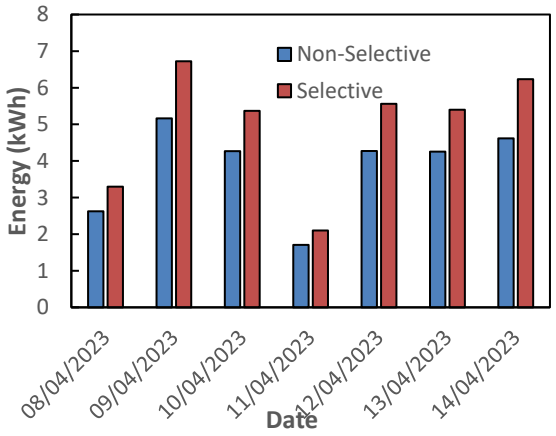

Fig. 10: Comparison of collector energy delivered per day at 0.038 m^3s^{-1} (80 CFM) or 0.015 $m^3s^{-1}m^{-2}$

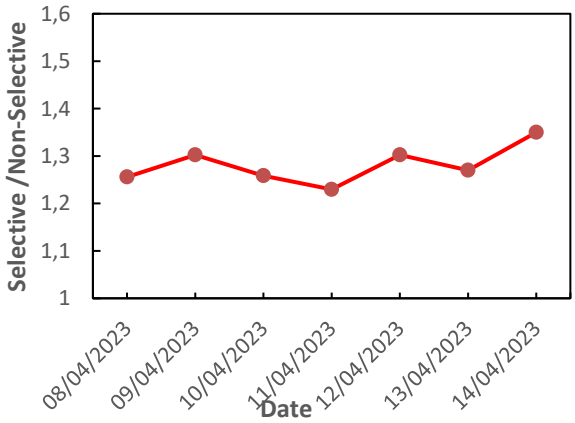

Fig. 11: Ratio of daily energy delivered for collector with selective absorber coating (i.e., low-emittance) relative to the non-selective (i.e., high-emittance)

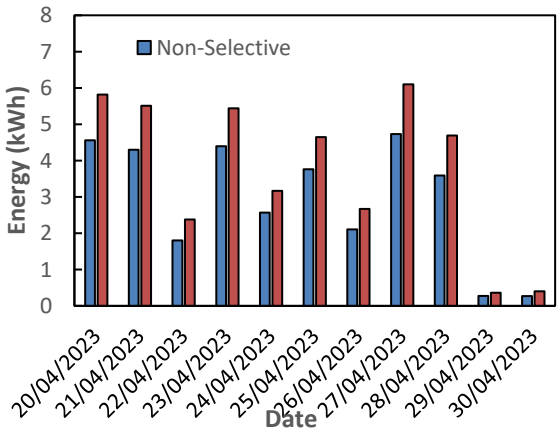

Fig. 12: Comparison of collector energy delivered per day at 0.050 m^3s^{-1} (105 CFM) or 0.02 $m^3s^{-1}m^{-2}$

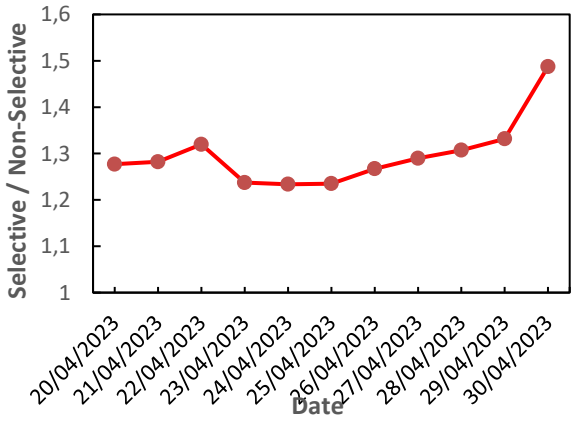

Fig. 13: Ratio of daily energy delivered for collector with selective absorber coating (i.e., low-emittance) relative to the non-selective (i.e., high-emittance)

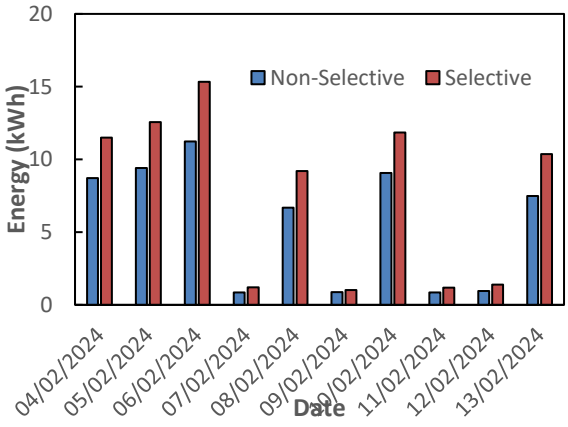

Fig. 15: Ratio of daily energy delivered for collector with selective absorber coating (i.e., low-emittance) relative to the non-selective (i.e., high-emittance)

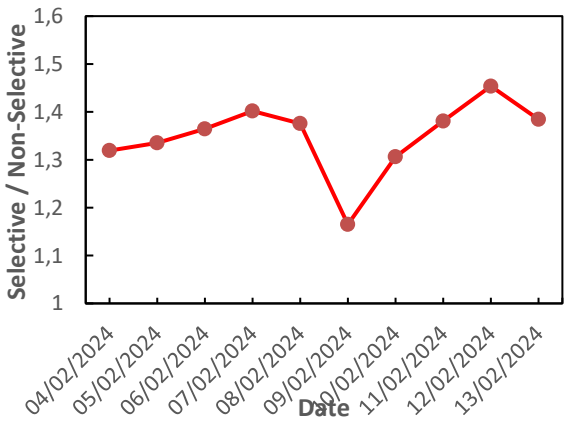

Fig. 14: Comparison of collector energy delivered per day at 0.087 m^3s^{-1} (185 CFM) or 0.035 $m^3s^{-1}m^{-2}$

In addition to the daily energy delivered, the efficiencies of the two solar air collectors are also compared with respect to the air flow rates, as illustrated in Figs. 16 and 17. The data used for the efficiency calculation were taken from clear sky sunny days, with the time frame at noon when the solar incidence angle is at its minimum.

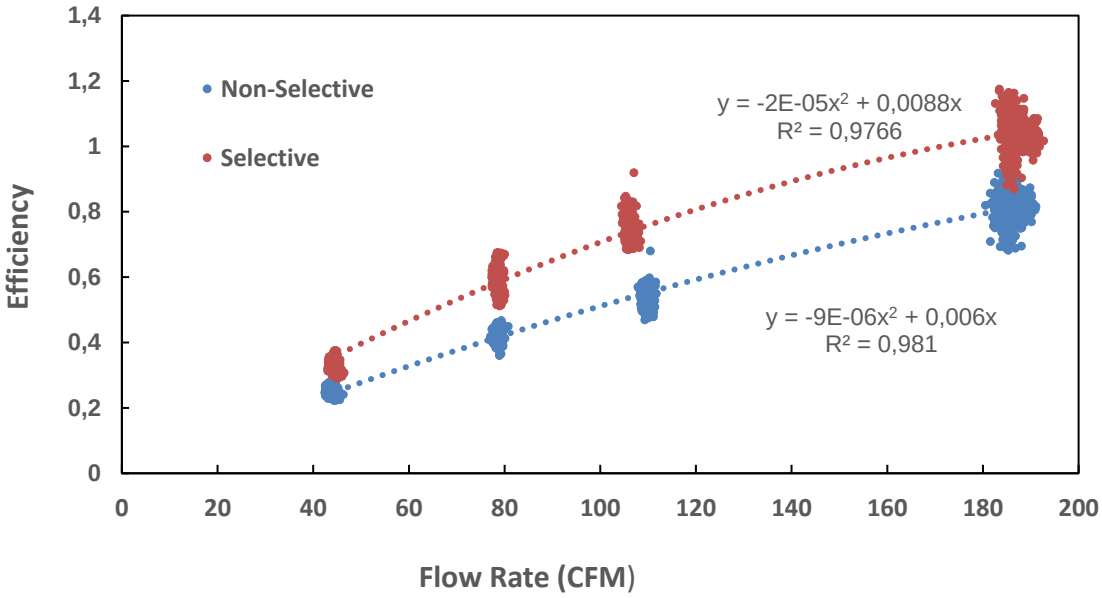

Fig. 16: Efficiencies of the two Solar Air Collectors at different Flow Rates

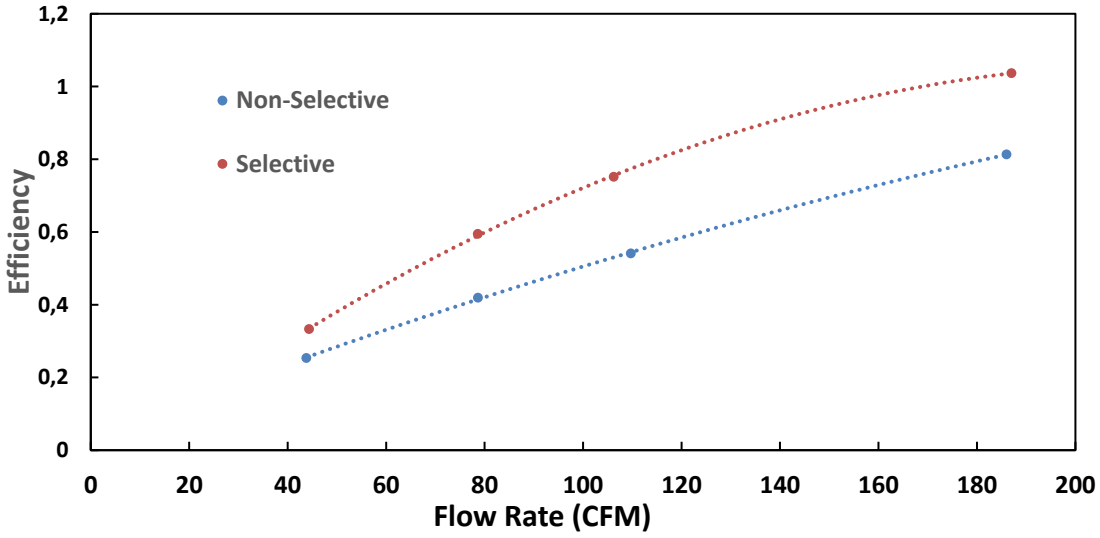

Fig. 17: Efficiencies of the two Solar Air Collectors at different Flow Rates (Average Values)

4. Conclusion

By comparing the energy delivered by the two solar air collectors, results indicated that the solar air collector with the low- emittance surface coating operated at higher efficiency and delivered air at higher temperature as compared to the collector with high-emissivity coating. Specifically, depending on operational conditions,

the energy ratios of the two collectors show that the solar collector with low emissivity surface coating delivered approximately 1.2 - 1.5 times the energy as the identical non-selective collector.

5. Acknowledgments

The authors gratefully acknowledge the financial support of Natural Resources Canada through the Office of Energy Research and Development – Energy Innovation Program (EIP). Collector samples were provided by Trigo Energies.

6. References

Badache, M., Rousse, D. R., Hallé, S., & Quesada, G., 2013. Experimental and numerical simulation of a two-dimensional unglazed transpired solar air collector. Solar Energy, 93, 209-219.

Shukla, A., Nkwetta, D.N., Cho, Y.J., Stevenson, V. and Jones, P., 2012. A state of art review on the performance of transpired solar collector. Renewable and Sustainable Energy Reviews, 16(6), pp.3975-3985.

SRCC, Solar Rating and Certification Corporation. 2016. Report OG-100 ICC-SRCC Certified Solar Air Heating Collector #. https://solar-rating.org/, accessed August 1, 2024.

SRCC, Solar Rating and Certification Corporation. 2020. Report OG-100 ICC-SRCC Certified Solar Air Heating Collector #10002111. https://solar-rating.org/, accessed August 1, 2024.

Fraunhofer-Institut für Solare Energiesysteme ISE, 2020. Test report according to EN 12975-1:2006+A1:2010 /EN ISO 9806:2017, Report KTB: 2020-02-k2.